

Article

The Glaze Icing Performance of a Robust Superhydrophobic Film Composed of Epoxy Resin and Polydimethylsiloxane

Aoyun Zhuang^{1,*}, Chao Li², Jianping Yu¹  and Yao Lu³

¹ Key Laboratory of Air-Driven Equipment Technology of Zhejiang Province, Quzhou University, Quzhou 324000, China

² Nanchang Power Supply Branch of State Grid Jiangxi Electric Power Co., Ltd., Nanchang 330069, China

³ Department of Chemistry, School of Physical and Chemical Sciences, Queen Mary University of London, London E1 4NS, UK

* Correspondence: 36118@qzc.edu.cn

Abstract: Ice accretion on transmission lines can cause operational difficulties and disastrous events. In this study, a micro/nano-structured epoxy resin/polydimethylsiloxane (EP/PDMS) film on glass, with water droplet contact angles (CA) observed as high as 160° and the water droplet sliding angle (SA) < 1° was fabricated by aerosol-assisted chemical vapor deposition (AACVD). The glaze icing performance of the superhydrophobic EP/PDMS films have been investigated by comparing the bare glass and room temperature vulcanized (RTV) silicon rubber-coated glass substrate representing the glass insulators and silicone rubber insulators, respectively. Compared with the bare glass and the RTV silicon rubber coating, the EP/PDMS superhydrophobic coating showed excellent performance in delaying glaze icing, especially in the early stages of icing. After 20 min of glaze icing with tilting angle of 90° at −5 and −10 °C, 38.9% and 85.7% of the RTV silicon rubber coating were covered, respectively, and less than 3% of the EP/PDMS coating was covered by ice when the blank glass sheet was completely covered. The EP/PDMS films also showed good mechanical robustness and long-term stability, which are important considerations in their widespread real-world adoption.

Keywords: glaze icing; superhydrophobic; robust; EP/PDMS; AACVD; RTV silicon rubber coating



Citation: Zhuang, A.; Li, C.; Yu, J.; Lu, Y. The Glaze Icing Performance of a Robust Superhydrophobic Film Composed of Epoxy Resin and Polydimethylsiloxane. *Coatings* **2023**, *13*, 1271. <https://doi.org/10.3390/coatings13071271>

Academic Editor: Hideyuki Murakami

Received: 17 June 2023

Revised: 9 July 2023

Accepted: 17 July 2023

Published: 20 July 2023



Copyright: © 2023 by the authors. Licensee MDPI, Basel, Switzerland. This article is an open access article distributed under the terms and conditions of the Creative Commons Attribution (CC BY) license (<https://creativecommons.org/licenses/by/4.0/>).

1. Introduction

The performance of the transmission line is directly related to the safe operation of the power grid. The construction of transmission lines in many areas has been facing the problem of icing on the transmission lines, which seriously threatens the safe operation of power grids [1,2]. Therefore, researching the anti-icing theory and methods for transmission lines and effectively suppressing the occurrence of icing on transmission line insulators has become a focus of attention and an urgent technical problem in the entire power industry [3].

A variety of methods have been developed to deal with the anti-icing and deicing problems of transmission line conductors, such as the ferromagnetic material method [4], AC /DC short circuit deicing method [5] and overcurrent deicing method [6]. However, due to the electrical insulation properties of transmission line glass insulators and their unique geometric structures, many methods suitable for transmission line wires cannot be applied to the surface of insulators. At present, the anti-icing and deicing methods applicable to the surfaces of insulators mainly include mechanical deicing methods [7–9] and anti-icing coating methods [10–12]. Mechanical deicing methods have the problems of extremely low safety and efficiency. At present, anti-icing coating methods mainly include photothermal coatings for anti-icing [13–16], electrothermal coatings for anti-icing [17–20], and hydrophobic coatings for anti-icing [21,22]. Photothermal coatings mainly rely on absorbing the energy of sunlight. When encountering continuous rainy weather or ice-covered transmission lines at night, photothermal coatings cannot absorb enough heat,

which greatly limits their anti-icing performance. If the electrothermal coating heats up for a long time, it will generate a lot of Joule heat. On the one hand, it will waste energy, and on the other hand, it will make the surface temperature of the coating higher and accelerate the aging of the coating, which is not conducive to its long-term use. Therefore, it is difficult to achieve a long-term anti-icing effect. The preparation of superhydrophobic anti-icing materials based on the surface of bionic lotus leaves has attracted the attention of many scholars and engineers [23–26]. It has great potential in the field of anti-icing of transmission lines, and it is currently a hot topic in this direction.

Although there are many methods for preparing superhydrophobic coatings [27–30], many methods are complicated in the preparation process and require sophisticated and expensive instruments. Although some of them have a simple preparation process, wear resistance of the film is not strong enough to be extended to practical applications [31,32]. At present, there are few superhydrophobic coatings with excellent wear resistance, and most of the microstructures of superhydrophobic coatings are easily damaged by external forces. In addition, the substrate materials used in many superhydrophobic coatings are difficult to apply due to the ultraviolet aging, acid rain corrosion and other factors. Therefore, it is of great significance to explore superhydrophobic coatings with excellent corrosion resistance and wear resistance, simple preparation processes and low costs. Aerosol-assisted chemical vapor deposition (AACVD) is a simple variant of CVD, mainly by ultrasonically atomizing a solution containing material precursors to generate an aerosol, which is then transported into a CVD reactor for reaction. Since the precursors of AACVD only need to be dissolved in a suitable medium, AACVD has obvious advantages over traditional CVD methods in terms of precursor availability. It has been successfully used to prepare a variety of materials, including various oxide coatings and polymer films [33–35].

In the previous paper published by our research group [31], a PTFE superhydrophobic transparent coating was successfully prepared in one step by the AACVD method. On this basis, we used epoxy resin as the raw material, and prepared micro–nano structures with excellent wear resistance without the need of other micro- or nano-structure particles. After low surface energy modification, a robust superhydrophobic EP/PDMS coating was prepared. The method has a simple preparation process and a high processing efficiency, and can meet the huge demand in the field of transmission lines. In addition, the raw material of the EP/PDMS coating is mainly ordinary epoxy resin, which is low in cost, and the materials and processes are environmentally friendly. Some of the previous studies on the anti-icing performance of superhydrophobic coatings were based on the freezing of static water droplets, which is quite different from the actual outdoor icing process. Therefore, in order to be closer to the natural conditions of the actual ice disaster, this paper uses an artificial climate laboratory to simulate the growth process of glaze icing on the coating surface. In this paper, the glaze icing test was carried out on the surface of the EP/PDMS superhydrophobic coating, and the influence of different sample tilt angles and freezing temperatures on the glaze icing was investigated. The anti-icing mechanism of the superhydrophobic surface was further analyzed.

2. Materials and Methods

2.1. Sample Preparation

The epoxy resin and triethylenetetramine (1.0:0.1 g) were combined and dissolved in methanol (20 mL). The reactor was assembled in a top-down heating configuration with a carbon heating block positioned above a plate supporting the substrate. Deliver the aerosol onto the heated substrate with N₂ (0.5 L/min). The reactor temperature was set at 290 °C and the deposition started, at which point the temperature was set to increase from 290 to 350 °C at a rate of 2 °C/min during the deposition. Once the entire EP precursor (20 mL) was aerosolized, the reactor temperature was cooled back to 290 °C, and the process was repeated again with dynamic temperature control for the second and third EP layers, finally yielding three layers of robust EP film.

The PDMS elastomer precursor and its curing agent (1.0:0.1 g) were combined and dissolved in ethyl acetate (50 mL) with stirring. The prepared EP film was immersed in the silicone elastomer and curing agent solution at room temperature for 5 min, and then heated at 250 °C for 5 min to finally obtain a superhydrophobic epoxy resin/polydimethylsiloxane (EP/PDMS) film (84.1 μm thickness). The process for the fabrication of EP/PDMS samples can be referred to our previous work [36]. The RTV silicon rubber-coated glass surface and bare glass substrate were prepared for comparison. The size of the selected area for sample is 30 mm \times 25 mm.

2.2. Test Platform

The glaze icing performance of samples was tested based on the artificial climate laboratory shown in Figure 1. The internal length of the artificial climate laboratory is 3.8 m, the internal diameter is 2 m, and the lowest temperature can drop to -45 °C, the minimum air pressure can be reduced to 34.6 kPa, and the maximum simulated wind speed can reach 3 m/s. The artificial climate test room is equipped with nozzles that meet IEC 60068 standard, which can produce water droplets with a diameter of 10–100 μm . During the icing process, the standard nozzle was fixed on the stainless steel bracket, the nozzle was aimed directly above the sample, and the water tank was placed in the artificial climate test room. In order to ensure that different samples have as close to the same test environment as possible, a sample bracket as shown in Figure 1 was designed. The bracket can change the angle to observe the icing results of samples under different angles. In addition, it is also possible to conduct icing tests on multiple different samples in one test, ensuring the consistency of humidity and temperature.

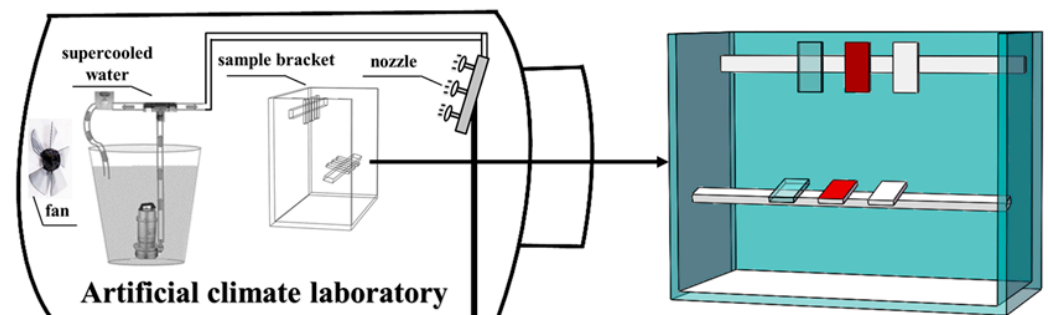


Figure 1. Schematic diagram of artificial climate laboratory and sample bracket.

2.3. Procedure

The icing test carried out in the artificial climate chamber includes the following three parts:

Prepare the supercooled water: mix deionized water and sodium chloride in a certain proportion, stir and dissolve thoroughly to prepare water with a conductivity of 255 $\mu\text{S}/\text{cm}$ (20 °C). The water tank was placed in an artificial climate test room to fully cool down to below 5 °C.

Glaze icing test: Fix the sample on the bracket and put it into the artificial climate laboratory, reduce the temperature of the artificial climate laboratory to -10 °C and leave it for 30 min, so that the temperature of the sample piece is reduced to the environment of the artificial climate laboratory. The temperature is consistent and meets the temperature conditions required for the glaze icing test. Then, maintain the temperature in the artificial climate test room, fix the standard nozzle on the stainless steel bracket, adjust the direction of the nozzle so that it is aligned directly above the sample, keep the distance between the nozzle and the sample at 0.5 m. The rainfall on the sample surface is controlled to be 90 L/h·m². Record the initial time of glaze icing as $t = 0$ min, and take pictures every 20 min. The ice-covered area of the sample surface was calculated using AutoCAD 2010 software, (Autodesk, San Rafael, CA, USA) (version 16.0).

Icing weight: Before the glaze icing, the weight of different samples was recorded. After the glaze icing test reaches the predetermined time, the ice completely frozen on the sample surface was weighed.

3. Results

3.1. Glaze Icing Performance at Different Tilt Angles

By setting the inclination angles of samples to 90° and 15°, respectively, the influence of the inclination angles on the glaze icing performance on the surface of samples with different wettability was investigated. The ambient temperature of the artificial climate laboratory was set at −5 °C, and blank glass slides, RTV silicon rubber coatings and EP/PDMS superhydrophobic coatings were selected as samples. The icing time was set at 60 min, and the images of the icing morphology of different samples were collected every 20 min after the glaze icing began, and the final icing samples were weighed.

Firstly, we analyzed the test results of glaze icing under the condition of ambient temperature of −5 °C and inclination angle of 15°. Figure 2 shows the glaze icing of the bare glass, RTV silicon rubber film and the superhydrophobic EP/PDMS film with a tilting angle of 15° at −5 °C. Figure 3 shows the icing area ratio at different times on the bare glass, RTV silicon rubber film and the superhydrophobic EP/PDMS film and ice weight after 60 min with a tilting angle of 15° at −5 °C. It can be seen that the blank glass and the RTV silicon rubber coating were quickly covered with ice at the beginning. The icing area of the blank glass sheet and the RTV silicone rubber coating surface reached the maximum (100%) in the first 20 min, and remained basically unchanged for the next 40 min, while the EP/PDMS coating surface showed a linear upward trend as a whole. After 20 min, the surface of the blank glass was completely covered by the ice layer and the ice layer on the surface was thicker. At this time, the surface of the RTV silicon rubber coating was also basically completely covered by the ice layer; the ice-covered area was as high as 94.9% and, at this time, only 14.5% of the surface of the EP/PDMS superhydrophobic coating was covered. Most of the water droplets on the surface of the coating were still liquid water droplets, which have not further condensed into ice particles on the surface of the superhydrophobic coating, which can also explain that the EP/PDMS superhydrophobic coating has an excellent ability to delay surface icing in the early stage of glaze icing test. In addition, with an increase in the glaze icing time, the proportion of the ice-covered area on the surface of RTV silicon rubber coating has reached 100% at 40 min, and the ice-covered thickness on the surface of the blank glass sheet and the surface of RTV silicon rubber coating is more than 3 mm. At this time, the proportion of the ice-covered area on the surface of the EP/PDMS superhydrophobic coating is only 48.8%. The droplets attached to the surface of the EP/PDMS superhydrophobic coating condensed into ice particles and gradually grew up, and the anti-icing performance of the superhydrophobic coating surface was reduced.

After the glaze icing test was carried out for 60 min, the ice thickness on the surface of the blank glass and the RTV silicon rubber coating surface further increased and the ice layer was relatively flat. At this time, the icing area of the EP/PDMS superhydrophobic coating increased to 68.9%, as the ice particles staying on the surface of the superhydrophobic coating in the early stage gradually grew, the ice on the surface of the EP/PDMS superhydrophobic coating was in the shape of cocoons or strings of pearls, most of which began to grow from the hydrophilic part and then spread to the surroundings. Even so, more than 30% of the surface of the superhydrophobic coating was not covered by ice particles after the glaze icing test. It can be seen from Figure 3 that the ice weights on the surface of the blank glass and the RTV silicon rubber coating after the glaze icing test are basically similar, which are 3.5 and 3.4 g, respectively, while the ice weight on the surface of the EP/PDMS superhydrophobic coating is 2.3 g, only 66% of the weight of the ice on the surface of the blank glass. Therefore, it can be concluded that the surface of the EP/PDMS superhydrophobic coating has a better ability to delay glaze icing than blank glass and RTV silicon rubber coatings at an ambient temperature of −5 °C and an inclination angle of 15°.

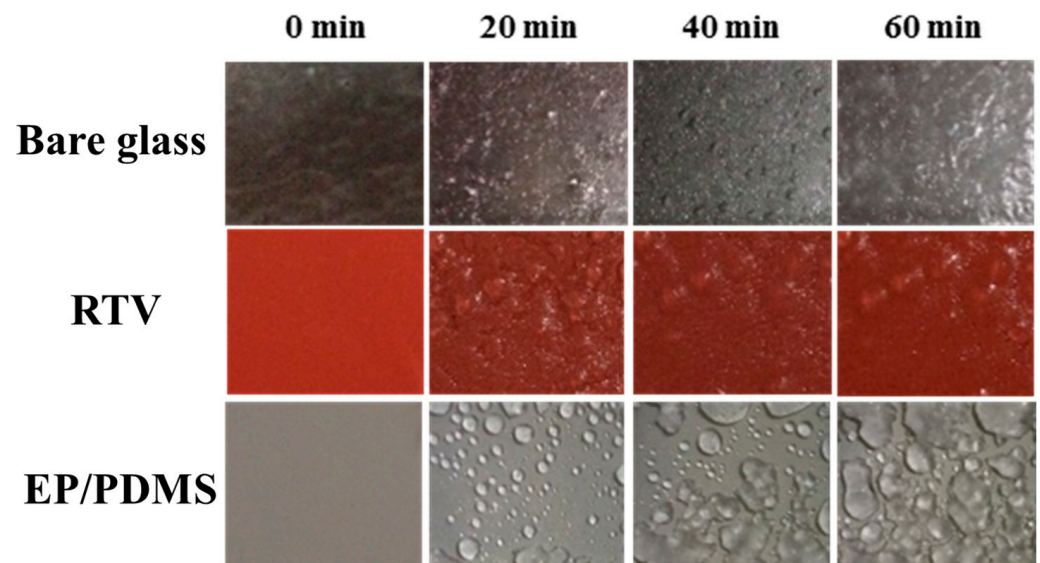


Figure 2. The glaze icing of the bare glass, RTV silicon rubber film and the superhydrophobic EP/PDMS film with tilting angle of 15° at -5°C .

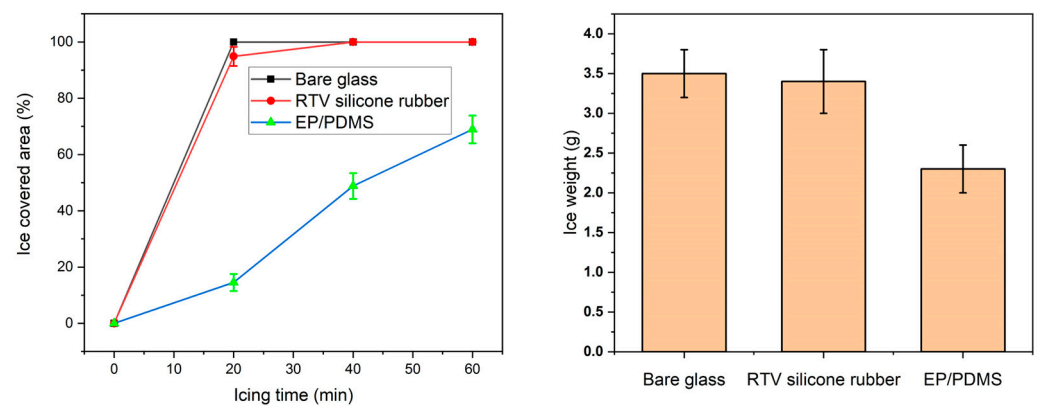


Figure 3. The icing area ratio at different times on the bare glass, RTV silicon rubber film and the superhydrophobic EP/PDMS film and ice weight after 60 min with tilting angle of 15° at -5°C .

Figure 4 shows the glaze icing of the bare glass, RTV silicon rubber film and the superhydrophobic EP/PDMS film with tilting angle of 90° at -5°C . Figure 5 shows the icing area ratio at different times on the bare glass, RTV silicon rubber film and the superhydrophobic EP/PDMS film and ice weight after 60 min with tilting angle of 90° at -5°C . It can be seen that the icing speed on the surface of the RTV silicon rubber coating slowed down compared to that at the inclination of 15° . The ice-covered area of the blank glass sheet still reached the maximum value (100%) in the first 20 min, and remained basically unchanged in the next 40 min, while the ice-covered area of the RTV silicon rubber coating and the EP/PDMS coating showed a linear upward trend as a whole, and the EP/PDMS coating exhibited a very slow rise rate. After 20 min, the ice-covered area on the surface of the blank glass reached 100%, while the ice-covered area on the surface of the RTV silicon rubber coating was only 38.9%. Only 2.6% of the surface of the EP/PDMS superhydrophobic coating was covered by water droplets, and most of the area remained dry and ice-free, which shows that the anti-icing effect of the EP/PDMS superhydrophobic coating was very obvious at an inclination angle of 90° . With an increase in glaze icing time, at 40 min, the ice-covered area on the surface of RTV silicon rubber coating reached 55.8%, and the ice particles on the surface gradually increased. At this time, there were only a small amount of small ice on the surface of EP/PDMS superhydrophobic coating. The icing area

was only 4.8%, which shows that the EP/PDMS superhydrophobic coating has excellent anti-icing performance compared with the blank glass and RTV silicon rubber coating.

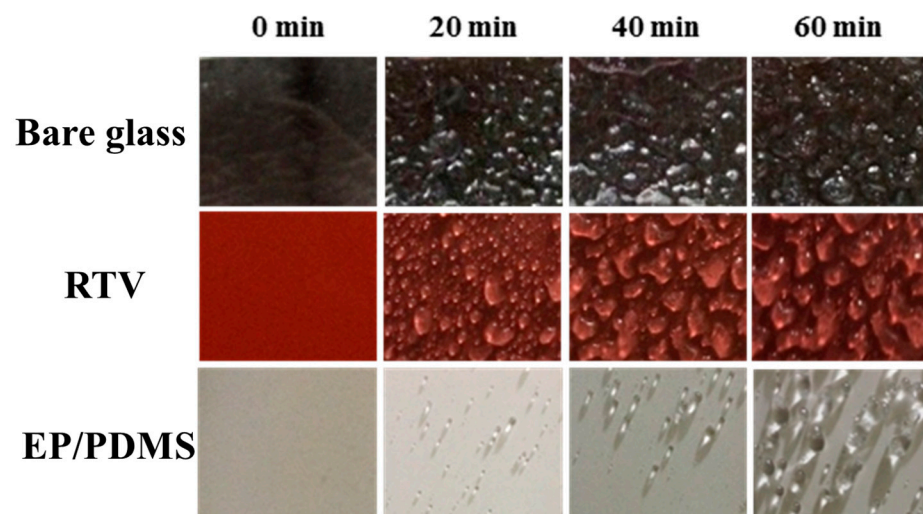


Figure 4. The glaze icing of the bare glass, RTV silicon rubber film and the superhydrophobic EP/PDMS film with tilting angle of 90° at -5°C .

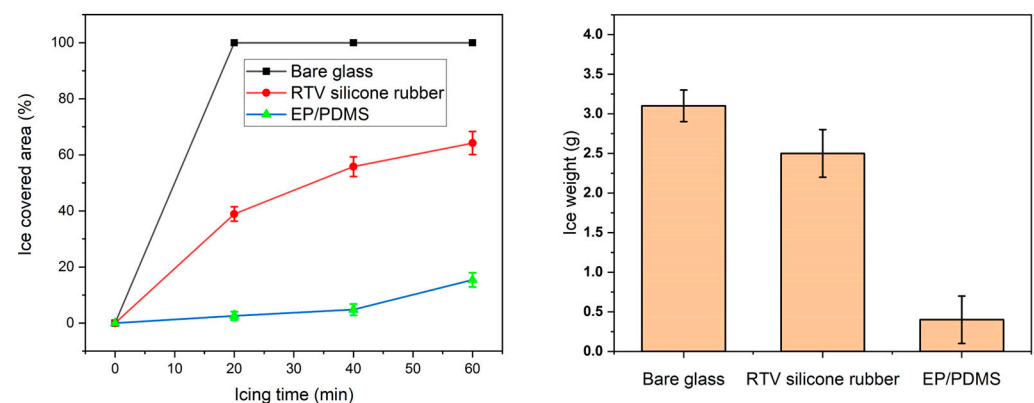


Figure 5. The icing area ratio at different times on the bare glass, RTV silicon rubber film and the superhydrophobic EP/PDMS film and ice weight after 60 min with tilting angle of 90° at -5°C .

After 60 min, the ice-covered morphology of the blank glass surface and the RTV silicon rubber coating was different from that of the surface with an inclination angle of 15° , and the surface ice layer presented a rougher morphology. The ice on the surface of the EP/PDMS superhydrophobic coating was scattered, and most of the area between the ice particles remained ice-free. The proportion of ice-covered area increased to 15.4%, accounting for only a quarter of the surface ice-covered area at an inclination angle of 15° . It can be seen from Figure 5 that compared with the icing results with an inclination of 15° , the ice weight on the surface of the sample has decreased, and the ice weight on the surface of the blank glass and the RTV silicon rubber coating after the test was 3.1 and 2.5 g, while the ice weight on the surface of the EP/PDMS superhydrophobic coating was 0.4 g, which is only 13% of the ice weight on the blank glass surface. Therefore, it can be shown that the inclination angle has a significant impact on the glaze icing results on the surface of the sample, and the EP/PDMS superhydrophobic coating showed a more significant anti-icing effect when the inclination angle of the sample was 90° .

The particle size of the EP/PDMS coating surface was basically distributed in the range of 200 nm–2 μm , and the small nanoparticles (diameter: 200–300 nm) made a significant contribution to the superhydrophobicity. According to the Cassie-Baxter model, the layered micro/nanostructures were able to form air entrapment under the water droplet, resulting

in a large contact angle. At the same time, under the modification of PDMS with low surface energy, the water droplet formed a small sliding angle with the surface. Due to the large contact angle formed by the water droplets on the surface, the heat transfer contact area between the water droplets and the surface was small, which can effectively slow down the heat transfer rate, so that the water droplets were not easy to freeze. In addition, the small contact area made the adhesion between the water droplet and the surface weak, making it easier for the water droplet to roll off the surface, preventing the water droplet from freezing on the surface. This not only prevented water droplets from freezing on the surface, but also rolled away other water droplets that stayed on the surface, thereby delaying the freezing of water droplets on the surface.

Due to the excellent bouncing properties of water droplets on the surface of the EP/PDMS superhydrophobic coating, the total time (also called contact time) from when the water drop first touches the surface of the superhydrophobic coating to when it completely detaches from the surface was greatly shortened compared with static contact, thus can greatly delay the condensation process of water droplets. Richard et al. [37] found in the study of the bouncing phenomenon of water droplets that when water droplets hit the surface of the superhydrophobic coating at different speeds of 20–230 cm/s, the contact time between the water droplet and the surface of the superhydrophobic coating is basically the same. This shows that within a certain speed range, there is no direct relationship between the impact speed of water droplets and the contact time, while the diameter of water droplets and the contact time are basically in a linear relationship. As the diameter of raindrops increases, the contact time between water droplets and the superhydrophobic coating surface gets longer. The diameter of the water droplets in the case of glaze icing in this paper was only about 100 μm , so the contact time between the water droplets and the surface of the superhydrophobic coating was very short. Since the tilt of 90° was the limit state, two angles of 15° and 60° were selected to illustrate the influence of the tilt angle on the surface icing. Figure 6 shows a schematic diagram of a water droplet bouncing on the superhydrophobic surface with tilting angles of 60° and 15° . During the process of the water droplet rolling from the same position to completely rolling off the surface, the number of water droplets colliding with the surface increases from two times at 60° to four times at 15° , the time for water droplets to stay on the surface becomes longer, and the probability of colliding with the defect area increases, which in turn increases the possibility of water droplets freezing on the surface.

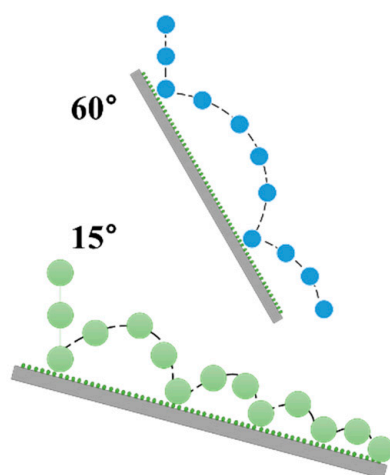


Figure 6. Schematic illustration of the water droplet bouncing on the superhydrophobic surface with tilting angles of 60° and 15° .

For the superhydrophobic sample surface of the same size, when the inclination angle of the superhydrophobic coating sample was small (15°), the lateral movement distance required for water droplets to bounce and roll off the superhydrophobic surface increased,

and the number of bouncing cycles increased. When more water droplets were on the superhydrophobic surface, and the contact time between the water droplets and the surface of the superhydrophobic coating was prolonged, and the water droplets were further cooled to increase the probability of ice, resulting in a larger amount of ice. However, when the inclination angle of the superhydrophobic coating sample became larger, the lateral movement distance required for water droplets to roll off the superhydrophobic surface became smaller, fewer water droplets existed on the superhydrophobic surface, and the shorter contact time also reduced the icing probability, resulting in less icing formation. In addition, water droplets on a surface with a large inclination angle are more likely to be carried away by other rolling water droplets due to their own gravity, making it less likely for water droplets to freeze on the surface.

3.2. Glaze Icing Performance under Different Ambient Temperatures

By selecting the sample inclination angle of 90° and changing the ambient temperature to -10°C , the glaze icing test was carried out and compared with the results of glaze icing at the ambient temperature of -5°C at the same sample inclination angle. Figure 7 shows the glaze icing of the bare glass, RTV silicon rubber film and the superhydrophobic EP/PDMS film with tilting angle of 90° at -10°C . Figure 8 shows the icing area ratio at different times on the bare glass, RTV silicon rubber film, and the superhydrophobic EP/PDMS film and ice weight after 60 min with a tilting angle of 90° at -10°C . It can be seen that when the temperature dropped to -10°C , the icing speed of the blank glass and the RTV silicon rubber coating surface increased to a certain extent compared with the temperature at -5°C . As the temperature decreased, the surface of the RTV silicone rubber coating was the same as that of the blank glass sheet, and the ice-covered area had basically reached the maximum in the first 20 min, and remained basically unchanged in the next 40 min. The ice-covered area of the EP/PDMS coating surface showed a linear upward trend in the first 40 min and maintained a low rate, and then there was a significant acceleration in the next 20 min. After 20 min, the surface of the blank glass was completely covered by ice, and the area of ice on the surface of RTV silicon rubber coating reached 85.7%, which was about 2.2 times the surface ice area under the condition of -5°C . This showed that the ambient temperature had a great influence on the result of glaze icing. At this time, only about 2.0% of the surface area of the EP/PDMS superhydrophobic coating was covered by water droplets, and most of the area remained ice-free, which was similar to the glaze icing result at -5°C . With an increase in icing time, at 40 min, the ice-covered area of the RTV silicon rubber coating surface reached 90.2%, and the ice-coated particles continued to grow. At this time, only a small amount of small ice particles appeared on the surface of the EP/PDMS superhydrophobic coating, and its ice-covered area was only 8.1%, which can reflect that the EP/PDMS superhydrophobic coating still had excellent anti-icing performance at low temperatures.

After 60 min, the surface of the blank glass showed a rough ice-covered form. When the temperature of the rime ice-covered test environment is -5°C , the supercooled water droplets still have enough time to roll off the surface after landing on the surface of the sample, and cannot condense into ice on the surface of the sample. When the temperature dropped to -10°C , the water droplets were further cooled during the process of spraying from the nozzle to the surface of the sample, and it was easy to freeze quickly to form an ice layer on the glass surface. Similarly, the surface of the RTV silicon rubber coating at this time was almost completely covered by the ice layer, while the surface of the EP/PDMS superhydrophobic coating was only covered with long strips of ice, the other parts remained ice-free, and the proportion of the ice-covered area increased to 41.1%. It can be seen from Figure 8 that compared with the temperature at -5°C , the ice weight on the surface of the sample increased. The ice weight on the surface of the blank glass and the RTV silicon rubber coating after the ice coating was 3.2 and 3.0 g, while the ice weight on the surface of the EP/PDMS superhydrophobic coating was 1.1 g. In general, the ambient temperature had a certain degree of influence on the icing results on the surface of the sample, and the

EP/PDMS superhydrophobic coating still had a good anti-icing effect when the tilt was 90° and the temperature was −10 °C.

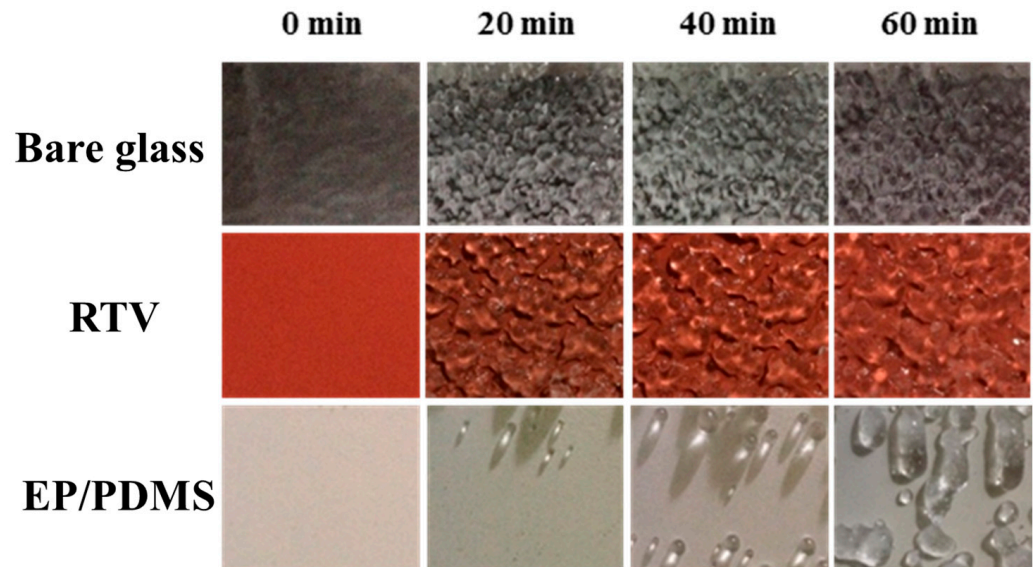


Figure 7. The glaze icing of the bare glass, RTV silicon rubber film and the superhydrophobic EP/PDMS film with tilting angle of 90° at −10 °C.

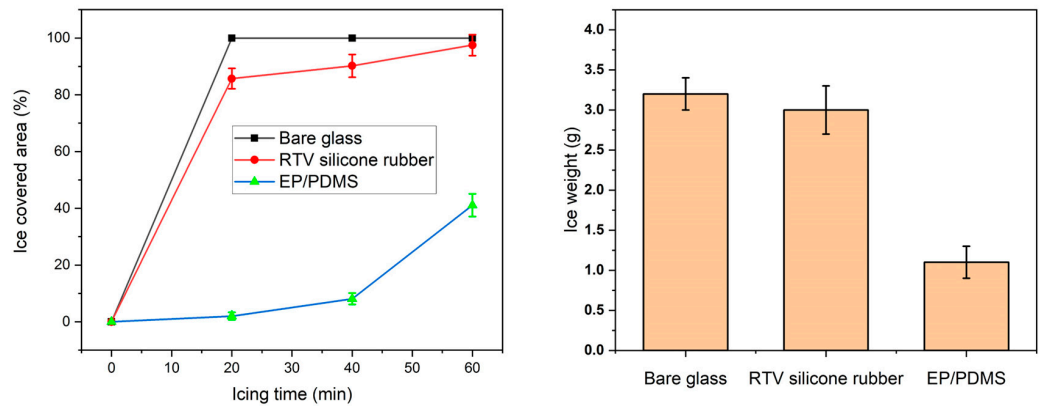


Figure 8. The icing area ratio at different times on the bare glass, RTV silicon rubber film and the superhydrophobic EP/PDMS film and ice weight after 60 min with tilting angle of 90° at −10 °C.

3.3. Ice Melting Performance

In order to compare the ice-melting performance of the sample coating after glaze icing, the ice-coated samples with an inclination of 90° and an ambient temperature of −10 °C were taken out of the artificial climate chamber and placed in a room temperature environment of 23 °C, and the sample was kept as the same inclined angle to observe the ice-melting process on the surface. Figure 9 shows the ice on the surface of samples after 5 min of melting. It can be seen from the figure that the surface of the blank glass was still covered by ice, and the melting speed was relatively slow. There were large particles of ice on the surface of the RTV silicon rubber coating. It had fallen off, leaving some small areas of ice, and the surface of the EP/PDMS superhydrophobic coating had no ice at all. It can be seen that the EP/PDMS coating had better self-recovery ability after the glaze icing.

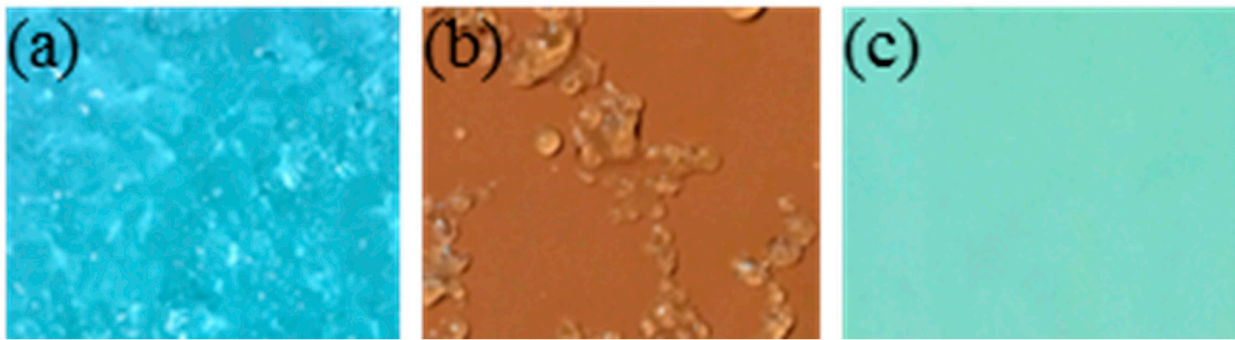


Figure 9. Ice melting on the bare glass (a), RTV silicon rubber film (b), and the superhydrophobic EP/PDMS film (c).

3.4. Insulation and Stability

The surface resistivity of the blank glass sheet, RTV silicone rubber coating and EP/PDMS superhydrophobic coating under direct current were $4.6 \times 10^{12} \Omega$, $2.2 \times 10^{13} \Omega$, and $5.2 \times 10^{14} \Omega$, respectively, and the surface resistivity of the blank glass sheet was the lowest among the three samples. The surface resistivity of the RTV silicone rubber coating was higher than that of the blank glass sheet, while the surface resistivity of the EP/PDMS superhydrophobic coating was about 5 times and 113 times that of the blank glass sheet and the RTV silicone rubber coating, respectively. The excellent insulating properties of EP/PDMS coatings are very important for the potential application of superhydrophobic coatings in transmission lines.

The sandpaper abrasion test was used to demonstrate the robustness of the EP/PDMS films. A 100 g weight was placed on a 26 mm \times 26 mm sample, the EP/PDMS film was brought into contact with the sandpaper, and the sample was moved back and forth on the sandpaper by an external force parallel to the substrate (rotating 90° every 25 cm). The contact angle of the film was still $>153^\circ$, and the sliding angle was $<4^\circ$ even after 5 m of abrasion, demonstrating that the robustness of the EP/PDMS film. Furthermore, the sample was placed at room temperature and irradiated with UV for 120 h (365 nm, 3.7 mW/cm²). After 120 h of UV irradiation, the contact angle of water droplets on the coating surface still reached 159° , and the sliding angle was less than 1° , showing the coating has excellent stability to UV radiation. After 100 static water droplet freezing cycles, the contact angle of water droplets on the surface of the EP/PDMS superhydrophobic coating decreased to 153.3° , and the sliding angle increased to 2.5° , demonstrating excellent stability in delayed icing. This is of great significance for the application and promotion of EP/PDMS superhydrophobic coatings in outdoor environments.

4. Discussions

Since the EP/PDMS superhydrophobic coating cannot ensure that its surface structure was completely uniform during the preparation process, there may be structural defects in some areas due to factors such as fluctuations in coating conditions, so that the structural requirements of the superhydrophobic coating cannot be met, resulting in weaker superhydrophobic properties in some regions. In addition, due to the unique micro-nano spherical structure of the superhydrophobic coating itself, compared with a flat coating, it was more susceptible to damage from external forces during long-term use, resulting in the formation of defect points. Since the pollution would continue to cover the surface of the superhydrophobic coating, and the some of the pollution showed a hydrophilic nature, it would also weaken the superhydrophobic performance of the EP/PDMS coating, resulting in the retention of supercooled water droplets, and then the droplets condensed into ice and trapped more droplets that grow around them. There was also a critical size limit for water droplets to roll off the surface of the superhydrophobic coating, some small water droplets were easy to stay on the surface of the superhydrophobic coating, and the water

droplets condensed into ice in a short time, and then formed superhydrophobic defect points near the small ice crystals.

In addition to the defect point factor, the hydrophobic properties of the EP/PDMS superhydrophobic coating surface will also change at low temperatures. It can be seen from Figure 10 that at room temperature, water droplets can be in the Cassie state on the surface of the EP/PDMS superhydrophobic coating, showing the shape of spherical water droplets, as shown in the picture on the left. As the surface temperature decreases, water vapor condenses and forms ice particles on the surface of the EP/PDMS superhydrophobic coating and the internal voids of the micro-nano structure as shown in the picture in the middle. The EP/PDMS coating was composed of micro/nano spherical particles, and the surface of the particles was covered by an ice layer, so the low surface energy characteristics of PDMS were greatly weakened, which in turn made the superhydrophobic properties of the EP/PDMS coating lose, making the coating from hydrophobic to hydrophilic. Finally, the dynamic balance of water droplets on the surface of EP/PDMS superhydrophobic coating was changed. The water droplets entered the micro-nano structures on the superhydrophobic surface to form a Wenzel state.

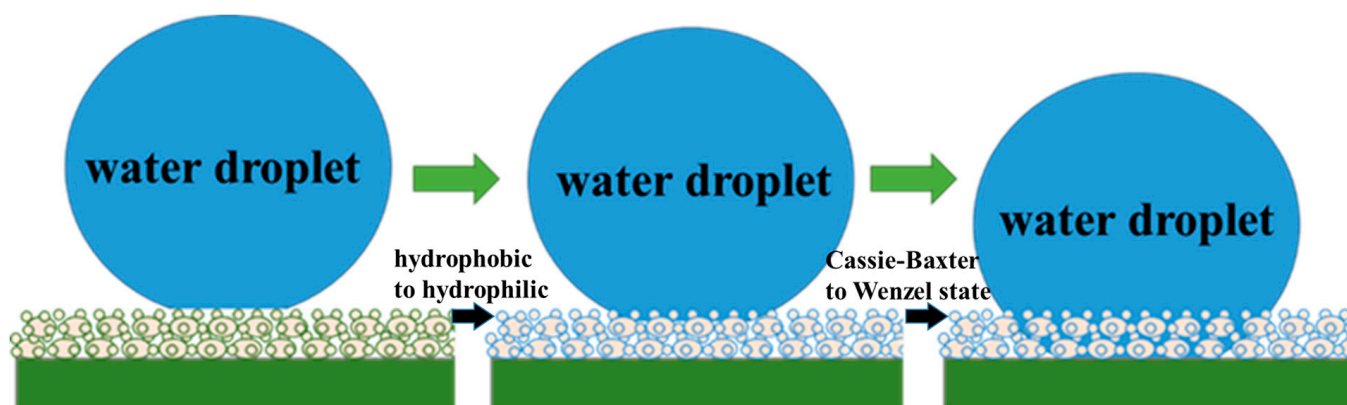


Figure 10. The transition from Cassie state to Wenzel state.

The freezing of water droplets on the surface of EP/PDMS superhydrophobic coating belonged to heterogeneous nucleation. Water molecules first formed crystal nuclei on the coating surface, and liquid-phase water continuously grew on the crystal nuclei. As the temperature of water droplets decreased, the supercooling degree of water droplets increased, the thermal motion of water molecules became slower, and the critical nucleation barrier decreased, which promoted water molecules to cross the critical nucleation energy barrier and then nucleate. According to the Fourier heat transfer law and the heat energy calculation formula, since the real solid–liquid contact area between the water droplet and the surface of the EP/PDMS superhydrophobic coating was much smaller than that of the blank glass sheet and the RTV silicone rubber coating, the heat transfer rate was also much lower. At the same time, the heat transferred between the water droplet and the superhydrophobic coating was very little, so the water droplet was not easy to freeze on the surface of the superhydrophobic coating.

In summary, the anti-icing mechanism of EP/PDMS superhydrophobic coating is summarized as follows: First of all, the contact area between the water droplet and the surface of the superhydrophobic EP/PDMS coating was small, the heat transfer between the water droplet and the coating was slow, and the temperature of the water droplet decreased slowly and was not easy to freeze. Secondly, after the supercooled water droplets hit the surface of the superhydrophobic coating, due to the rough structure and low surface energy of the coating itself, the adhesion between the water droplets and the coating was small, and there were repeated bounces between the water droplets and the superhydrophobic coating, shortening the contact time between water droplets and the coating, thereby delaying the freezing process of water droplets on the surface of the superhydrophobic coating. However, due to the existence of surface defect points due to the preparation

process and other external conditions, there would be some areas with weak anti-icing performance in the superhydrophobic coating.

5. Conclusions

Superhydrophobic EP/PDMS films with micro/nanoparticles were successfully prepared on glass slides by an aerosol-assisted chemical vapor deposition method through a dynamic temperature control process which resulted in small nanoparticles embedded in and well protected by the microstructure. Through the glaze icing test, it was found that the EP/PDMS superhydrophobic coating exhibited excellent ability to delay the icing under different inclination angles and different ambient temperatures. When the glass surface and the RTV silicone rubber coating surface were almost completely covered by ice, only less than 3% of the EP/PDMS coating surface was covered. The superhydrophobic EP/PDMS film had outstanding performance in terms of wear resistance, and it can still maintain good superhydrophobic performance after being worn on sandpaper for 5 m. In addition, it also had excellent electrical insulation performance and weather resistance, combined with low cost and environmental friendliness, it is expected to expand applications in transmission lines, building exterior walls, and other household and industrial fields.

Author Contributions: Conceptualization, A.Z.; writing—original draft preparation, A.Z.; writing—review and editing, C.L. and Y.L.; supervision, J.Y. and Y.L. All authors have read and agreed to the published version of the manuscript.

Funding: This research received no funding.

Institutional Review Board Statement: Not applicable.

Informed Consent Statement: Not applicable.

Data Availability Statement: The data used to support the findings of this study are available from the corresponding author upon request.

Conflicts of Interest: The authors declare no conflict of interest.

References

1. Dong, B.; Jiang, X.; Yin, F. Development and prospect of monitoring and prevention methods of icing disaster in China power grid. *IET Gener. Transm. Distrib.* **2022**, *16*, 4480–4493. [[CrossRef](#)]
2. Tao, B.; Cheng, L.; Wang, J.; Zhang, X.; Liao, R. A review on mechanism and application of functional coatings for overhead transmission lines. *Front. Mater.* **2022**, *9*, 995290. [[CrossRef](#)]
3. Wang, Y. Numerical study of a droplet impact on cylindrical objects: Towards the anti-icing property of power transmission lines. *Appl. Surf. Sci.* **2020**, *516*, 146155. [[CrossRef](#)]
4. Zheng, W.; Teng, L.; Lai, Y.; Zhu, T.; Li, S.; Wu, X.; Cai, W.; Chen, Z.; Huang, J. Magnetic responsive and flexible composite superhydrophobic photothermal film for passive anti-icing/active deicing. *Chem. Eng. J.* **2022**, *427*, 130922. [[CrossRef](#)]
5. Wang, J.; Fu, C.; Chen, Y.; Rao, H.; Xu, S.; Yu, T.; Li, L. Research and Application of DC De-Icing Technology in China Southern Power Grid. *IEEE Trans. Power Deliv.* **2012**, *27*, 1234–1242. [[CrossRef](#)]
6. Jiang, X.; Fan, C.; Xie, Y. New method of preventing ice disaster in power grid using expanded conductors in heavy icing area. *IET Gener. Transm. Distrib.* **2019**, *13*, 536–542. [[CrossRef](#)]
7. Endres, M.; Sommerwerk, H.; Mendig, C.; Sinapius, M.; Horst, P. Experimental study of two electro-mechanical de-icing systems applied on a wing section tested in an icing wind tunnel. *CEAS Aeronaut. J.* **2017**, *8*, 429–439. [[CrossRef](#)]
8. Zhou, J.Z.; Lai, S.W.; Xu, X.P.; Chen, Y.H.; Chu, W.J.; Gao, Y.M. R&D of Equipment for Deicing by Thermal Water-Jet and Mechanical Deicing Method. *Appl. Mech. Mater.* **2012**, *268–270*, 1288–1293. [[CrossRef](#)]
9. Zhang, Z.; Chen, B.; Lu, C.; Wu, H.; Wu, H.; Jiang, S.; Chai, G. A novel thermo-mechanical anti-icing/de-icing system using bi-stable laminate composite structures with superhydrophobic surface. *Compos. Struct.* **2017**, *180*, 933–943. [[CrossRef](#)]
10. Liu, Y.; Xu, R.; Luo, N.; Liu, Y.; Wu, Y.; Yu, B.; Liu, S.; Zhou, F. All-Day Anti-Icing/De-Icing Coating by Solar-Thermal and Electric-Thermal Effects. *Adv. Mater. Technol.* **2021**, *6*, 202100371. [[CrossRef](#)]
11. Cao, Y.; Lu, Y.; Liu, N.; Li, Y.; Wang, P.; Dai, C.; Wei, Y. Multi-applicable, durable superhydrophobic anti-icing coating through template-method and chemical vapor deposition. *Surf. Interfaces* **2022**, *32*, 102100. [[CrossRef](#)]
12. Zhu, T.; Cheng, Y.; Huang, J.; Xiong, J.; Ge, M.; Mao, J.; Liu, Z.; Dong, X.; Chen, Z.; Lai, Y. A transparent superhydrophobic coating with mechanochemical robustness for anti-icing, photocatalysis and self-cleaning. *Chem. Eng. J.* **2020**, *399*, 125746. [[CrossRef](#)]
13. Jiang, G.; Chen, L.; Zhang, S.; Huang, H. Superhydrophobic SiC/CNTs Coatings with Photothermal Deicing and Passive Anti-Icing Properties. *ACS Appl. Mater. Interfaces* **2018**, *10*, 36505–36511. [[CrossRef](#)] [[PubMed](#)]

14. Zhao, Z.; Chen, H.; Zhu, Y.; Liu, X.; Wang, Z.; Chen, J. A robust superhydrophobic anti-icing/de-icing composite coating with electrothermal and auxiliary photothermal performances. *Compos. Sci. Technol.* **2022**, *227*, 109578. [[CrossRef](#)]
15. Zhao, Y.; Yan, C.; Hou, T.; Dou, H.; Shen, H. Multifunctional Ti(3)C(2)T(x) MXene-Based Composite Coatings with Superhydrophobic Anti-icing and Photothermal Deicing Properties. *ACS Appl. Mater. Interfaces* **2022**, *14*, 26077–26087. [[CrossRef](#)]
16. Jiang, G.; Liu, Z.; Hu, J. Superhydrophobic and Photothermal PVDF/CNTs Durable Composite Coatings for Passive Anti-Icing/Active De-Icing. *Adv. Mater. Interfaces* **2021**, *9*, 202101704. [[CrossRef](#)]
17. Yan, S.; Zhou, X.; Zhang, H.; Dong, S.; Li, X.; Jiang, J.; Cao, X. Correction to: HVOF-Sprayed AlSi50 Alloy Coatings as a Novel Electrothermal Anti-icing/De-icing System for Polymer-based Composite Structures. *J. Therm. Spray Technol.* **2021**, *31*, 658–658. [[CrossRef](#)]
18. Wang, Z.; Zhu, Y.; Liu, X.; Zhao, Z.; Chen, J.; Jing, X.; Chen, H. Temperature self-regulating electrothermal pseudo-slippery surface for anti-icing. *Chem. Eng. J.* **2021**, *422*, 130110. [[CrossRef](#)]
19. He, Z.; Xie, H.; Jamil, M.I.; Li, T.; Zhang, Q. Electro-/Photo-Thermal Promoted Anti-Icing Materials: A New Strategy Combined with Passive Anti-Icing and Active De-Icing. *Adv. Mater. Interfaces* **2022**, *9*, 202200275. [[CrossRef](#)]
20. Sullivan, A.; Duan, X.; Yang, J. Energy-efficient anti-icing performance of a hybrid superhydrophobic and electrothermal coating on metallic substrates. *Mater. Chem. Phys.* **2023**, *301*, 127700. [[CrossRef](#)]
21. Wang, Z.-J.; Kwon, D.-J.; Lawrence DeVries, K.; Park, J.-M. Frost formation and anti-icing performance of a hydrophobic coating on aluminum. *Exp. Therm. Fluid Sci.* **2015**, *60*, 132–137. [[CrossRef](#)]
22. Wei, C.; Jin, B.; Zhang, Q.; Zhan, X.; Chen, F. Anti-icing performance of super-wetting surfaces from icing-resistance to ice-phobic aspects: Robust hydrophobic or slippery surfaces. *J. Alloys Compd.* **2018**, *765*, 721–730. [[CrossRef](#)]
23. Huang, X.; Sun, M.; Shi, X.; Shao, J.; Jin, M.; Liu, W.; Zhang, R.; Huang, S.; Ye, Y. Chemical vapor deposition of transparent superhydrophobic anti-icing coatings with tailored polymer nanoarray architecture. *Chem. Eng. J.* **2023**, *454*, 139981. [[CrossRef](#)]
24. Liang, B.; Zhang, G.; Zhong, Z.; Huang, Y.; Su, Z. Superhydrophilic Anti-Icing Coatings Based on Polyzwitterion Brushes. *Langmuir* **2019**, *35*, 1294–1301. [[CrossRef](#)] [[PubMed](#)]
25. Farhadi, S.; Farzaneh, M.; Kulinich, S.A. Anti-icing performance of superhydrophobic surfaces. *Appl. Surf. Sci.* **2011**, *257*, 6264–6269. [[CrossRef](#)]
26. Ruan, M.; Li, W.; Wang, B.; Deng, B.; Ma, F.; Yu, Z. Preparation and anti-icing behavior of superhydrophobic surfaces on aluminum alloy substrates. *Langmuir* **2013**, *29*, 8482–8491. [[CrossRef](#)]
27. Li, X.M.; Reinhoudt, D.; Crego-Calama, M. What do we need for a superhydrophobic surface? A review on the recent progress in the preparation of superhydrophobic surfaces. *Chem. Soc. Rev.* **2007**, *36*, 1350–1368. [[CrossRef](#)]
28. Simpson, J.T.; Hunter, S.R.; Aytug, T. Superhydrophobic materials and coatings: A review. *Rep. Prog. Phys.* **2015**, *78*, 086501. [[CrossRef](#)]
29. Jeevahan, J.; Chandrasekaran, M.; Britto Joseph, G.; Durairaj, R.B.; Mageshwaran, G. Superhydrophobic surfaces: A review on fundamentals, applications, and challenges. *J. Coat. Technol. Res.* **2018**, *15*, 231–250. [[CrossRef](#)]
30. Zaman Khan, M.; Militky, J.; Petru, M.; Tomková, B.; Ali, A.; Tören, E.; Perveen, S. Recent advances in superhydrophobic surfaces for practical applications: A review. *Eur. Polym. J.* **2022**, *178*, 111481. [[CrossRef](#)]
31. Zhuang, A.; Liao, R.; Dixon, S.C.; Lu, Y.; Sathasivam, S.; Parkin, I.P.; Carmalt, C.J. Transparent superhydrophobic PTFE films via one-step aerosol assisted chemical vapor deposition. *RSC Adv.* **2017**, *7*, 29275–29283. [[CrossRef](#)]
32. Zhuang, A.; Yang, L.; Zhao, X.; Guo, C.; Zuo, Z.; Yuan, Y. Facile Fabrication of Transparent Superhydrophobic Film Based on PTFE by One-Step Hot Melting Process. *J. Nanosci. Nanotechnol.* **2016**, *16*, 9867–9869. [[CrossRef](#)]
33. Claros, M.; Setka, M.; Jimenez, Y.P.; Vallejos, S. AACVD Synthesis and Characterization of Iron and Copper Oxides Modified ZnO Structured Films. *Nanomaterials* **2020**, *10*, 471. [[CrossRef](#)] [[PubMed](#)]
34. Mokrushin, A.S.; Gorban, Y.M.; Averin, A.A.; Gorobtsov, P.Y.; Simonenko, N.P.; Lebedinskii, Y.Y.; Simonenko, E.P.; Kuznetsov, N.T. Obtaining of ZnO/Fe(2)O(3) Thin Nanostructured Films by AACVD for Detection of ppb-Concentrations of NO(2) as a Biomarker of Lung Infections. *Biosensors* **2023**, *13*, 445. [[CrossRef](#)] [[PubMed](#)]
35. Mehanna, Y.A.; Upton, R.L.; Crick, C.R. Highly rough surface coatings via the ambient temperature deposition of thermosetting polymers. *J. Mater. Chem. A* **2019**, *7*, 7333–7337. [[CrossRef](#)]
36. Zhuang, A.; Liao, R.; Lu, Y.; Dixon, S.C.; Jiamprasertboon, A.; Chen, F.; Sathasivam, S.; Parkin, I.P.; Carmalt, C.J. Transforming a Simple Commercial Glue into Highly Robust Superhydrophobic Surfaces via Aerosol-Assisted Chemical Vapor Deposition. *ACS Appl. Mater. Interfaces* **2017**, *9*, 42327–42335. [[CrossRef](#)]
37. Richard, D.; Clanet, C.; Quere, D. Contact time of a bouncing drop. *Nature* **2002**, *417*, 811. [[CrossRef](#)] [[PubMed](#)]

Disclaimer/Publisher's Note: The statements, opinions and data contained in all publications are solely those of the individual author(s) and contributor(s) and not of MDPI and/or the editor(s). MDPI and/or the editor(s) disclaim responsibility for any injury to people or property resulting from any ideas, methods, instructions or products referred to in the content.